IRAQI JOURNAL OF APPLIED PHYSICS
Vol. 22, No. 1, January-March 2026, pp. 62-76

Impact of i-Layer Thickness on Band Alignments of a-Si:H Solar Cells: A Simulation Study Using SCAPS Software

Saba A. Obaid [1]
Fouad A. Senaed [2]
Burak Y. Kadem [3*]

[1] Department of Physics, College of Science, University of Babylon, Babylon, IRAQ
[2] Ishtar Medical Institute, Ministry of Higher Education and Scientific Research, Baghdad, IRAQ
[3] College of Science, Al-Karkh University of Science, Baghdad, IRAQ
* Corresponding author: drburakkadem@gmail.com

Energy band alignments regarding amorphous silicon solar cells are assessed using SCAPS-1D software both under illumination and in dark. We looked at how the thickness of the extrinsic and intrinsic layers affected the band bending as well as alignment of the energy bands, as well as how they affected solar cell performance. Several thicknesses of the intrinsic layer are used, starting from 10nm to 60nm, while the extrinsic layer's thickness stays fixed and symmetric in all devices (20, 30, 40, 50, 60, 70, and 80nm). The study indicates that appropriate PIN thickness adjustment can enhance performance and adaptability in amorphous silicon solar cells. Higher thicknesses are also used, and comparisons are introduced based on the band bending, Fermi level position, splitting, and depletion region width observed. The band bending has shown different behavior based on different PIN thicknesses. Solar cell results show a dependence behavior on the PIN thickness and the depletion region width The device with a thickness of 180 nm (i = 80 nm, N = 50 nm, and P = 50 nm) and a JSC of 14.4 mA/cm^2, open circuit voltage of 1.03 V, an FF of 77.1%, and a PCE of 11.4% is shown to have the best performance. The performance of thicker PIN solar cells is obviously decreased.

Keywords: Solar cells; Fermi level; a-Si:H; Energy bands; SCAPS-1D
Received: 13 May 2025; Revised: 15 July 2025; Accepted: 22 July 2025; Published: 1 January 2026

1. Introduction

Silicon is an exceedingly favorable substance in the domain of solar energy owing to its abundance as the most prevalent semiconductor in the Earth's crust. In general, Si semiconducting wafers dominate approximately 95% of the market for solar cells. Nevertheless, the drawback of employing Si in flexible solar cells lies in its brittleness, making it susceptible to breakage under bending stress [1]. Over the course of several decades, research was done on hydrogenated amorphous silicon (a-Si:H), which made it one of the potential materials for solar cells [2]. This reputation is ascribed to its favorable characteristics, such as a large direct bandgap (E_g=1.70-1.80eV) that results in a high absorption coefficient as well as a lower deposition temperature process that allows for a wider variety of substrate material options than crystalline silicon (c-Si) [2]. For devices like batteries [5], solar cells [4], and transistors [3], a-Si:H semiconductor is technologically crucial. Because of its adjustable conduction type and low defect density, it was widely used in photovoltaic (PV) applications over the years [6]. The radial distribution function [7] describes how the configurations regarding silicon as well as hydrogen in 3D space are directly related to the optoelectronic advantages it provides. The limited flexibility of flexible solar cells made of a-Si presents difficulties. For improving power conversion efficiency (PCE) of such devices, research in this domain is essential. The flexible a-Si solar cell is thought to be a viable way to increase the specific power (kW/kg) of solar cell while resolving the production cost issues related to crystalline silicon (c-Si). Using lightweight materials as well as flexible manufacturing methods might help achieve a higher specific power, which is especially important for space applications [8]. Beginning in the early 1990s, researchers have worked on circuit models for a-Si solar cells, moving from basic studies of the carrier properties in a-Si cells to the development of basic circuit models. The circuit model for a-Si solar cells had gradually been improved over time due to developments in solar technology. A more advanced circuit model for amorphous Si solar cells was proposed in the year 1998 [9,10] using standard diode I-V index characteristics. Utilizing semiconductor PN junctions' PV effect, PV cells transform light energy into electrical energy. A photocurrent (I_{ph}), an equivalent shunt diode, and circuit parasitic resistors make up the equivalency circuit model for solar cells depicted in Fig. (1) [11].

In case of comparison with other solar cell types, flexible a-Si photovoltaic cells have special material and structural properties. Light-induced carriers in the solar cell only experience drift motion rather than diffusion because of the a-Si's disordered crystal structure, which leads to an incredibly low carrier diffusion length. In order to mitigate occurrence of pure tunnel current in the PN junction, a thicker intrinsic

layer is regularly added between P-layer and N-layer [10]. A PIN diode structure is produced as a result of this technique (see Fig. 1). Wang and colleagues have lately created foldable crystalline Si (c-Si) wafers, which are renowned for their strong light-harvesting properties [10]. Since c-Si is a semi-conductor with indirect optical bandgap, there's a trade-off between thickness and efficiency of light harvesting, even though increasing flexibility frequently entails decreasing wafer thickness. They were able to reduce a 160µm wafer's thickness to 60µm. The resultant wafer showed good flexibility, but because of its glossy surface, which reflected almost 30% of the incident sunlight, it was not appropriate for solar cell fabrication. Additionally, thin-film (~300nm) a-Si:H solar cells have shown a notable PCE of 7% for large-scale modules and 10% for lab-scale cells [12]. Allowing light to penetrate the intrinsic region is one of the PIN device's crucial parameters. This must be considered in the photodiode's physical design in order to maximize light collecting. In current simulation study, improving solar cell performance requires adjusting intrinsic layer that is crucial for charge carrier properties. Generally, a-Si:H differs from c-Si primarily due to its atomic disorder, which results in a much shorter carrier diffusion length. Consequently, a-Si:H solar cells have a narrower depletion region. To overcome this limitation, an i-layer is inserted between the p- and n-layers. In the PIN structure, the i-layer is fully depleted and establishes an internal electric field, enabling efficient carrier transport by drift rather than diffusion [13]. A single PIN-based a-Si solar cell structure is suggested. A very thin extrinsic layer and a thicker i-layer with thicknesses of around 20 nm and 500 nm is used, respectively, have been suggested by Benigno and co-authors [13]. As a result, we have suggested several PIN layer thicknesses. A thin PIN junction and a variety of intrinsic layer thicknesses are used to create a flexible a-Si: H solar cell.

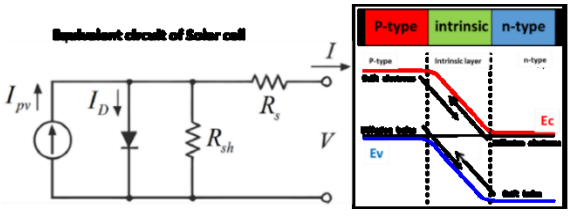

Fig. (1) The equivelant circuit of a solar cell and the band energy allignment of PIN junction

2. Simulated Solar Cell Structure

In the past, performances of several solar cell types have been simulated by using SCAPS-1D software. Idda and Ayat achieved an efficiency of 11.93% by simulating a solar cell made of a-Si: H/c-SiGe using SCAPS-1D [14]. Additionally, Belarbi et al. used SCAPS-1D to model the characteristics of a ZnSe/CdS/CIGS/Si solar cell, achieving a 24.94% efficiency [15]. The device structure of a-Si: H PIN solar cells that had been used in the present research has been based on utilizing symmetric extrinsic layers (N and P layers) with thicknesses ranging between 20 nm and 60 nm and altering the i-layer thickness from 10 to 80 nm. Through altering i-layer thickness, PIN solar cell's efficiency could be increased [16]. The thickness of i-layer influences the energy band (EB) alignment in a PIN solar cell; adding an i-layer between P and N layers enhances performance of a PIN solar cell in comparison to a PN cell [13]. Another research found that adding a hetero i-layer to PIN solar cell improved the cell's PCE and carrier lifetime [17]. Furthermore, enhanced performance of solar cells was achieved by optimizing double-i-layer thickness and band gap in a-Si:H/c-Si:H PIN solar cells [18]. Open circuit voltage (V_{OC}), short circuit current density (J_{SC}), PCE, and fill factor (FF) are some of the components that make up solar cell characteristics. Larger values of such parameters are necessary to achieve higher PCE because these characteristics primarily determine PV performance of solar cells [19]. In this case, i-layer's presence is essential in affecting the alignment of the energy levels, which in turn affects the device voltage. Photogenerated carriers must be removed without experiencing recombination loss in order for the device performance to be improved. As a result, the carrier diffusion (drift) length limits the solar cell's FF [20]. The solar cell's FF and PCE were determined with the use of the next equations [21]:

$$\text{PCE}\ (\%) = \frac{J_{max} V_{max}}{P_{in}} \quad (1)$$

$$\text{FF} = \frac{J_{max}\, V_{max}}{J_{sc}\, V_{oc}} \quad (2)$$

where P_{in} represents incident light power and J_{max} (mA/cm^2) and V_{max} (V) represent current density and voltage at maximum power output point in J-V curves, respectively

3. Results and Discussion

3.1. Extrinsic layer thickness (20nm)

The change in the i-layer thickness results in different energy band (EB) gradient of the PIN structure in dark and under illumination. Figure (2) shows the EB alignment of a PIN with different i-layer thicknesses. For a very thin PIN structure, there is no band bending in the EB alignment and the EB gradient is almost linear in dark and under illumination. Because of the thinner i-layer as well as the distribution of charge carriers for both extrinsic layers, Fermi level (E_f) at 10 nm and 20 nm of i-layer thickness is separated in the dark at interface of i-layer with P- and N-layers, creating a small depletion region [22]. The i-layer thickness and charge carrier distribution affect the size of the depletion layer in both extrinsic layers [23–24]. Whereas the distribution of charge carriers influences the potential landscape and may cause a deviation from the expected scaling of the depletion width with bias

voltage, a thinner i-layer produces a smaller depletion region [24]. The thickness and characteristics of the i-layer affect E_f splitting in the dark at the interface of intrinsic and extrinsic layers in a PIN system. For both extrinsic and intrinsic semiconductors, Ueno and Yang discovered that E_f pinning vanishes at a specific semiconductor sheet thickness [25]. They demonstrated that the thickness of semiconductor films and substrate work function control ultimate E_f position [22]. Luo et al. investigated the E_f pinning at metal/n-SiGe interfaces and found that the dominant mechanism of E_f pinning is intrinsic rather than extrinsic [18].

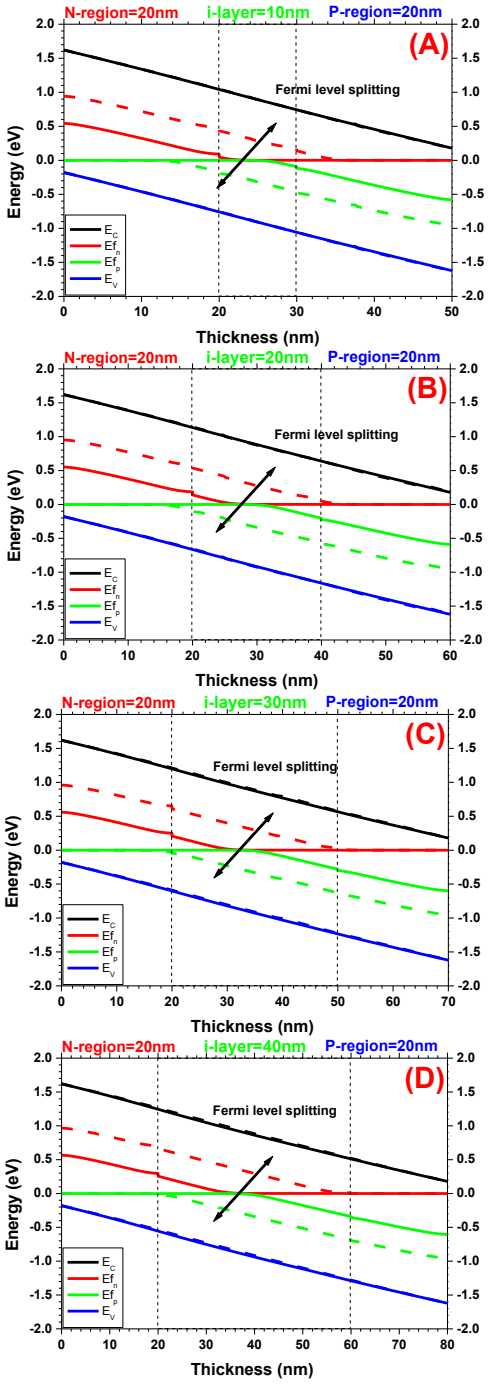

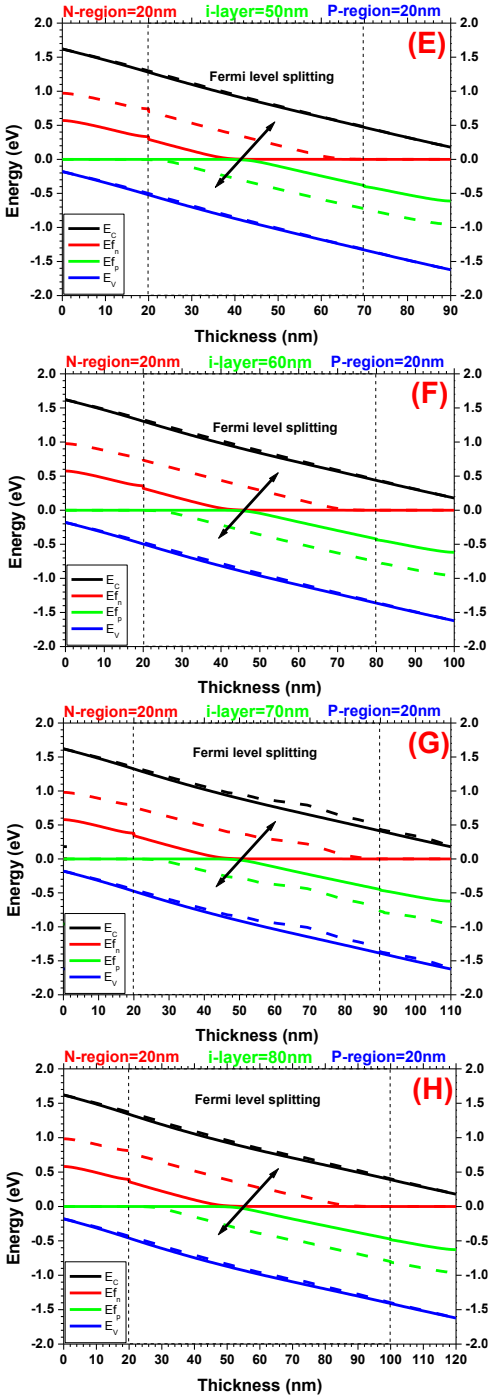

Fig. (2) Energy band alignments for a-Si: H-based PIN device with different i-layer thickness, (A) 10nm, (B) 20 nm, (C) 30nm, (D) 40 nm, (E) 00nm, (F) 60 nm, (F) 70nm and (G) 80 nm with symmetric N and P-layers thickness of 20nm. The solid lines represent level of energy in dark and dash lines represent energy level under illumination

In a PIN solar cell, i-layer plays a critical role in enhancing performance by acting as a buffer between the p-type and n-type layers. This layer reduces carrier recombination and facilitates efficient collection of photo-generated charges [17]. No change in band gap value is observed in all samples; however, change in E_f position is noticed under illumination, especially at

higher i-layer thickness. Under illumination, VB and CB shifted up slightly inside the depletion layer and increasing E_f splitting [26], resulting in separate E_{fn} and E_{fp}. The change in EB bending can be attributed to the carrier concentration distribution [22]. Under illumination, the photogenerated carriers increase the carrier density within the i-layer; this has resulted in increase the carriers' density and alter the charge distribution within the device, particularly near the edges of the depletion region [27]. At i-layer thickness more than 100nm, the EB demonstrate a small gradient and band bending. Usually, the grading of EB within the PIN diode, is associated with the varying doping levels across the different regions of the device. The graded EB decreases charge recombination due to mismatched energy levels and improves carrier separation and transport [28]. There is no discernible potential in the depletion region while it is dark, but as the distance between E_{fp} and E_{fn} increases, figure (2) illustrates a potential of roughly 0.7V inside the depletion region under illumination. Charge carrier transportation in the solar cells benefits from this capability. PCE, which primarily relies on the diffusion, generation, transportation, and collection of charge carriers by electrodes, determines solar cell performance [29]. Moreover, another crucial factor that affects solar cell's overall efficiency is metal-semiconductor contact and energy offset between CB and VB [30]. Figure (3A) exhibits J-V characteristics of studied solar cells under illumination with different i-layer and 20nm thicknesses of the extrinsic layers. Results are revealed that the overall performance enhances by increasing i-layer thickness. The use of nanoscale thickness is essential in this study as the main goal is to fabricate flexible a-Si solar cell. Therefore, increasing the thickness is critical factor and an optimize thickness must be proved. The thinner solar cells in this section is 50nm thickness, the thicker solar cell is 120nm thickness. As seen in Fig. (3B), a solar cell with i-layer thickness of 10nm achieves a higher V_{OC} of 1.08 Volt, while solar cell with i-layer thickness of 80nm exhibits the lowest value of 1.04 Volt. This decrease can be related to the previously indicated difference in E_f position. A single junction solar cell that is based upon a-SiC:H demonstrated a V_{OC} of 0.99V, as confirmed by Yunaz et al. [31]. According to Fischer et al. [32], a-Si: H single junction solar cells have V_{OC} of approximately 1 V. V_{OC} is mostly calculated with the use of the next relation [33] to compare the E_f of p-type (E_{fp}) and n-type (E_{fn}) semiconductors under open circuit conditions:

$$V_{OC} = \frac{E_{fn} - E_{fp}}{q} \qquad (3)$$

The FF of these devices shows high value of 82.7% for i-layer of 50nm thickness based solar cell and demonstrates slight decrease associated with decreasing i-layer thickness.

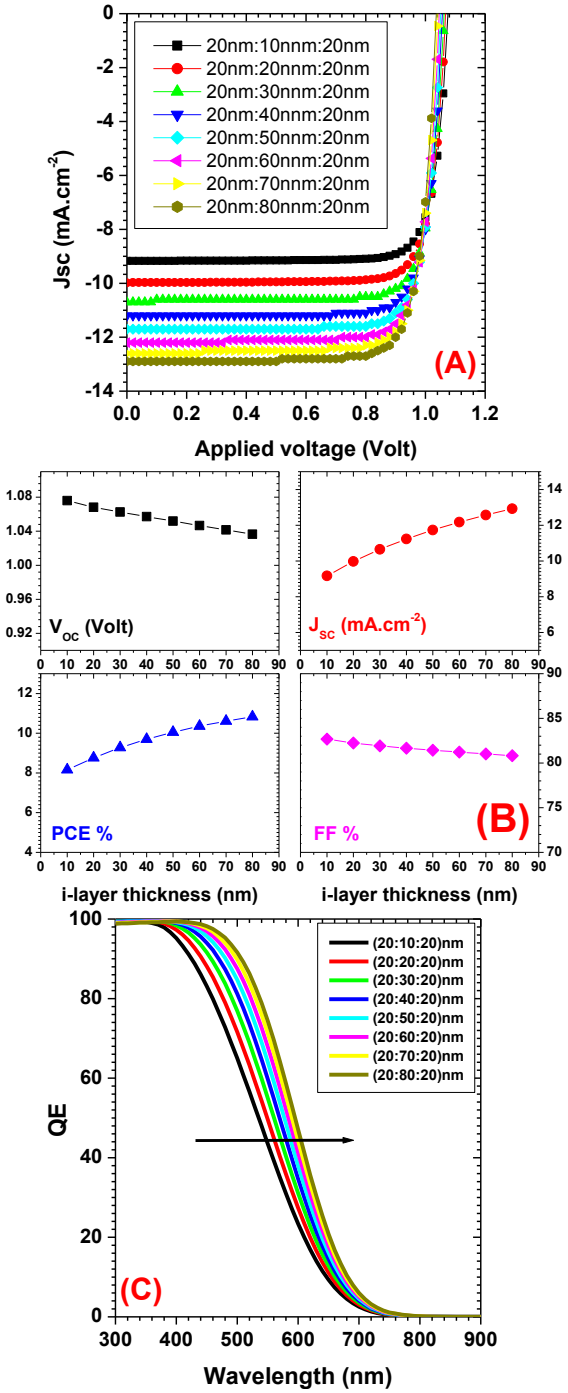

Fig. (3) Solar cell characteristics for a-Si: H-based PIN solar cell that has been symmetric extrinsic layers (20nm thickness and different i-layers), (A) J-V curve under illumination (B) Solar cell parameters and (C) QE

On the other hand, in an i-layer solar cell with an 80 nm thickness, the J_{SC} lead to 12.9 mA/cm^2. As illustrated in Fig. (3C), this increase is ascribed to the devices' rising quantum efficiency (QE) as i-layer thickness increases. PCE increased from 8.16% in i-layer of 10nm thickness based solar cell to reach as high as 10.83% in i-layer of 80nm thickness based solar cell. This is attributed to enhancement in the internal electric field resulting from fully depleted i-layer, permitting

efficient carrier transport [13].

3.2. Extrinsic layer thickness (30nm)

In the presented section, i-layer thickness varied from 10nm to 80nm and the extrinsic layers' thickness is fixed at 30nm. Results illustrated in Fig. (4) show that in dark, the depletion region is also generated inside the i-layer and the splitting of CB, VB and E_f is exhibited at all thicknesses.

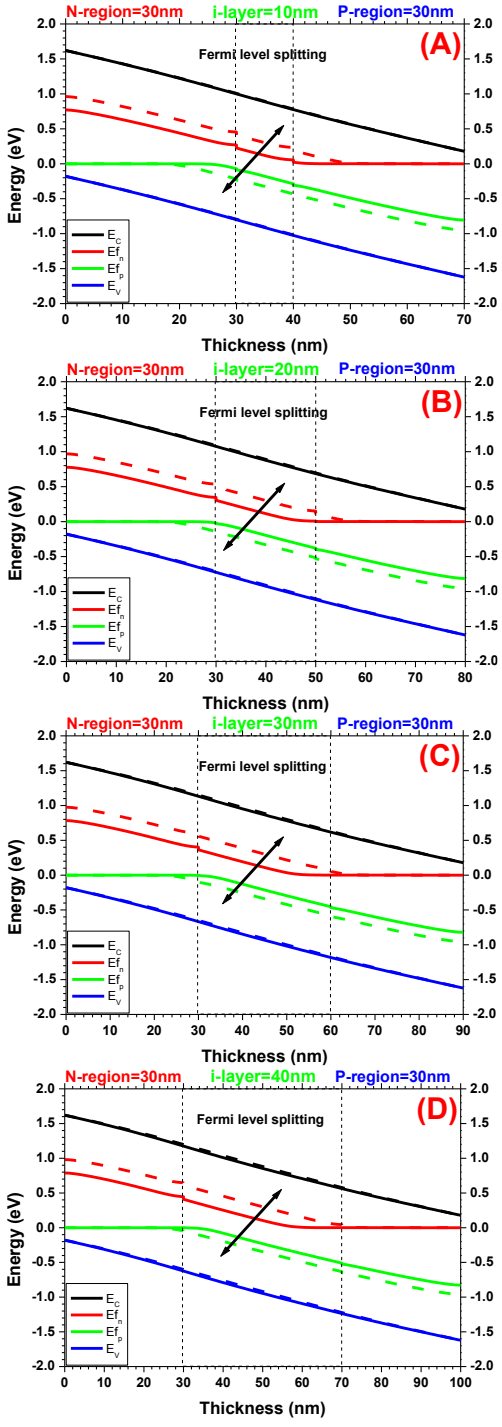

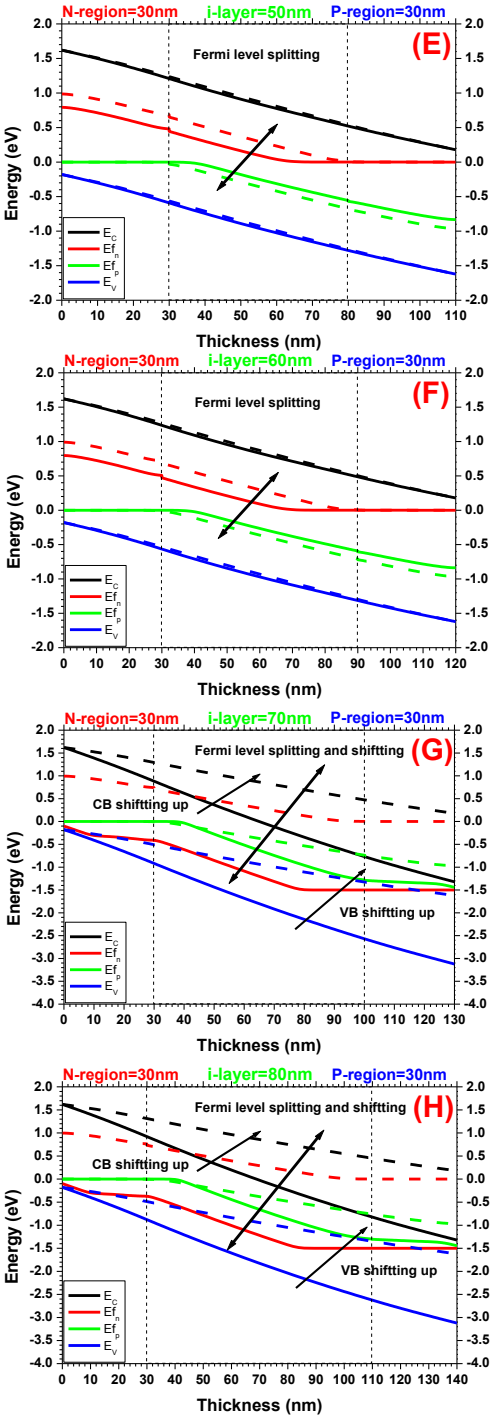

Fig. (4) Energy band alignments for a-Si:H-based PIN device with different i-layer thickness, (A) 10nm, (B) 20 nm, (C) 30nm, (D) 40 nm, (E) 50nm, (F) 60 nm, (F) 70nm and (G) 80nm with symmetric N and P-layers thickness of 30nm. The solid lines represent energy level in dark and the dash lines represent energy level under illumination

Under illumination, E_{fn} shifts from its original position toward CB and E_{fp} shifts toward VB. Moreover, no clear shifting in CB and VB is observed. At 130nm thickness based solar cell (N-layer is 30nm, i-layer is 70nm and P-layer is 30nm) and 140nm thickness based solar cell (N-layer is 30nm, i-layer is

80nm and P-layer is 30nm), all the energy levels (CB, VB and E_f) shift up resulting in low gradient energy bands. This is explained by the rise in photogenerated carriers, which causes a region to become completely depleted [26]. Additionally, it has been noted that EB alignment is significantly affected by the changes in the extrinsic layer thickness. The splitting of E_f inside the depletion region varies in the dark and under illumination, according to a comparison of results in figures (2C-H) and (4A-F). This might be explained by the distribution of charge carriers inside the depletion region, particularly following illumination when the number of photogenerated carriers increased [26]. An interesting pattern in the energy band alignment is observed at the 130 nm and 140 nm thicknesses of PIN-based solar cells as the band bending is different where the CB, VB and EF are shifting up noticeably.

Although no explicit explanation is given, the author suggests the following explanations: Fermi levels of holes (E_{fp}) and electrons (E_{fn}) are closer to VB and CB, respectively, in a dark environment. This is mostly because of the middle PIN's i-layer thickness, which has a balanced electron and hole concentration. The author recommends the following for similar outcomes: A concentration gradient of carriers is created toward the center of i-layer due to P-layer (positive) contributing some holes and the N-layer (negative) contributing some electrons. An electric field is created as a result of establishment of a space charge region. Here, E_f modifies itself to achieve equilibrium through counteracting the diffusion of carriers with the electric field produced by space charge region. In this equilibrium state, E_{fn} is closer to VB. While, under Illumination, upon photon absorption, charge carriers in the i-layer is generated, electrons move towards CB, and holes move towards VB. This movement reduces the concentration gradient in the i-layer and E_f adjusts to this new condition by moving closer to CB.

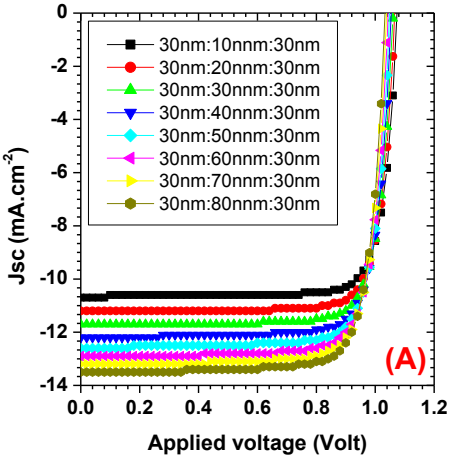

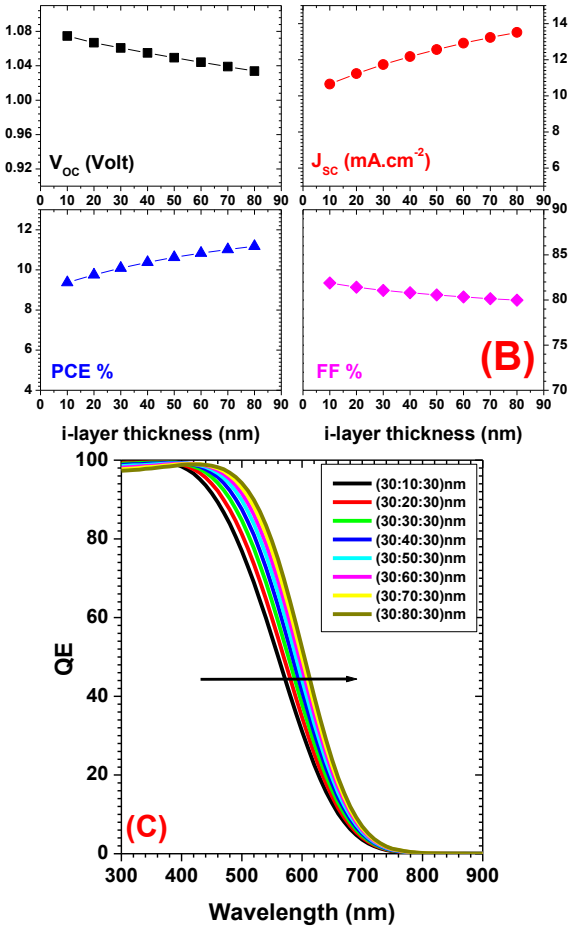

Fig. (5) Solar cell characteristics for a-Si:H-based PIN solar cell with symmetric extrinsic layers (30nm thickness and different i-layers), (A) J-V curve under illumination (B) Solar cell parameters and (C) QE

Figure (5A) exhibits J-V characteristics of studied solar cell under illumination with different i-layer and 30nm thicknesses of the extinct layers. Results have indicated that overall solar performance of cells enhances by the increase of i-layer and extrinsic layers' thicknesses. The best device performance is found for the PIN thickness of 140nm with V_{OC} of 1.03 V, J_{SC} of 13.52 mA/cm^2, FF of 80% and PCE of 11.18% as seen from Fig. (5B). Although, V_{OC} and FF are slightly decreased but the current density is increased, this increase is attributed to the enhancement in QE spectra shown in Fig. (5C). As i-layer thickness, the current increased and the absorption bands red shifted resulting in higher absorption.

3.3. Extrinsic layer thickness (40nm)

Figure (6) illustrates the use of a greater extrinsic layer thickness and a further increase in the i-layer thickness. CB has shown behavior in the dark that is comparable to the findings in Fig. (4G and H). The E_f is splitting inside the i-layer and there is no band bending. As seen in Fig. (6), CB displayed a distinct energy position at the interface with the front contact.

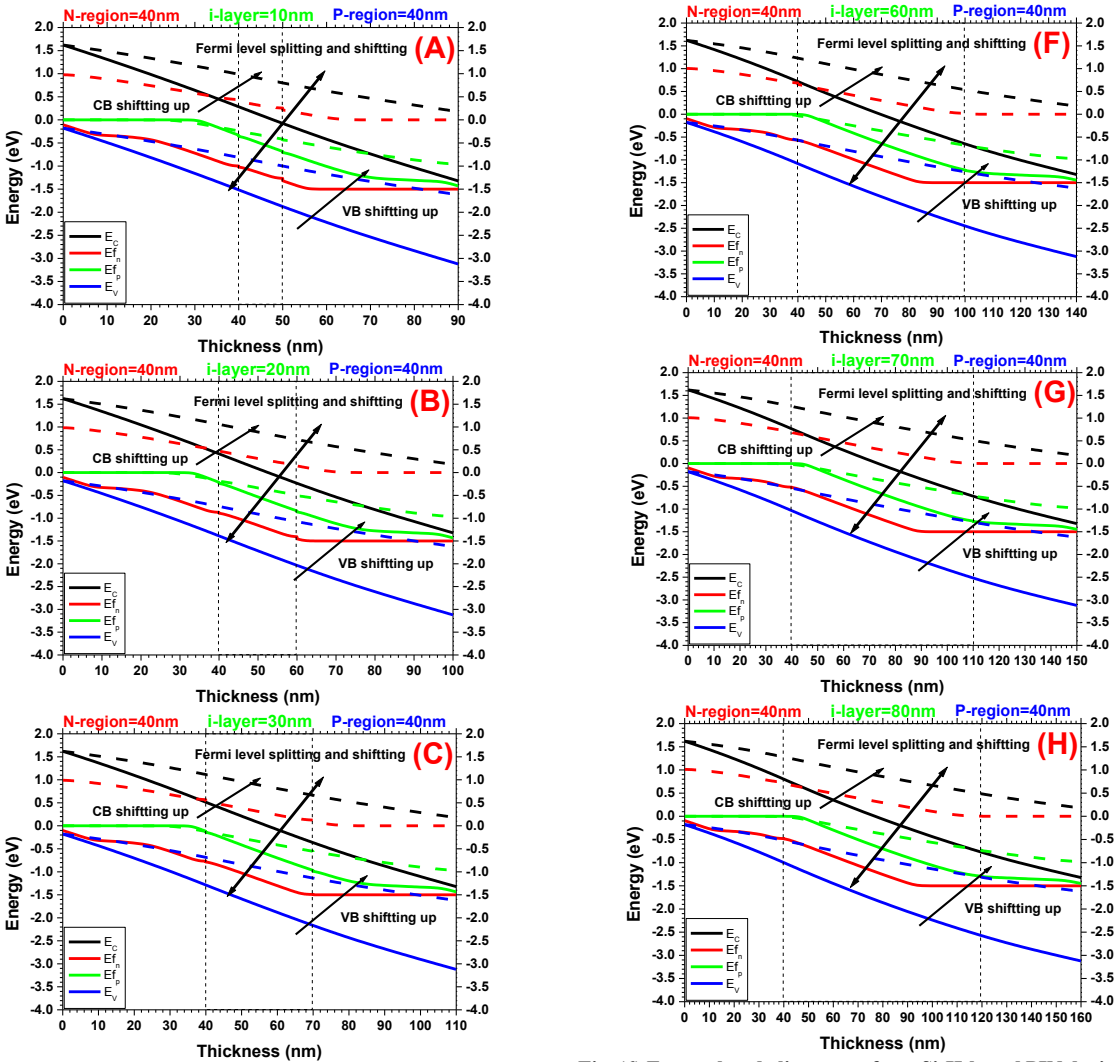

Fig. (6) Energy band alignments for a-Si:H-based PIN device that has different i-layer thickness, (A) 10nm, (B) 20 nm, (C) 30 nm, (D) 40nm, (E) 00 nm, (F) 60nm, (F) 70nm and (G) 80 nm with symmetric N and P-layers thickness of 40nm. The solid lines represent energy level in dark and the dash lines represent energy level under illumination

Under illumination, both CB and VB shifted up and EB become almost fully depleted device due to increasing the photogenerated carriers [26]. Similar behavior where the E_{fn} is close to VB and E_{fp} is close to CB is observed for these samples in dark. Whereas under illumination, E_{fn} moves close to CB and E_{fp} moves close to VB. The solar cell characteristics illustrated in Fig. (7A) show that the overall behavior is enhanced when increasing i-layer thickness. With a PIN thickness of 160nm, a J_{SC} of 14 mA/cm^2, V_{OC} of 1.04 V, a PCE of 11.37%, and an FF of 79%, the device performs at its optimum. The devices' increased QE is the cause of the current density increase.

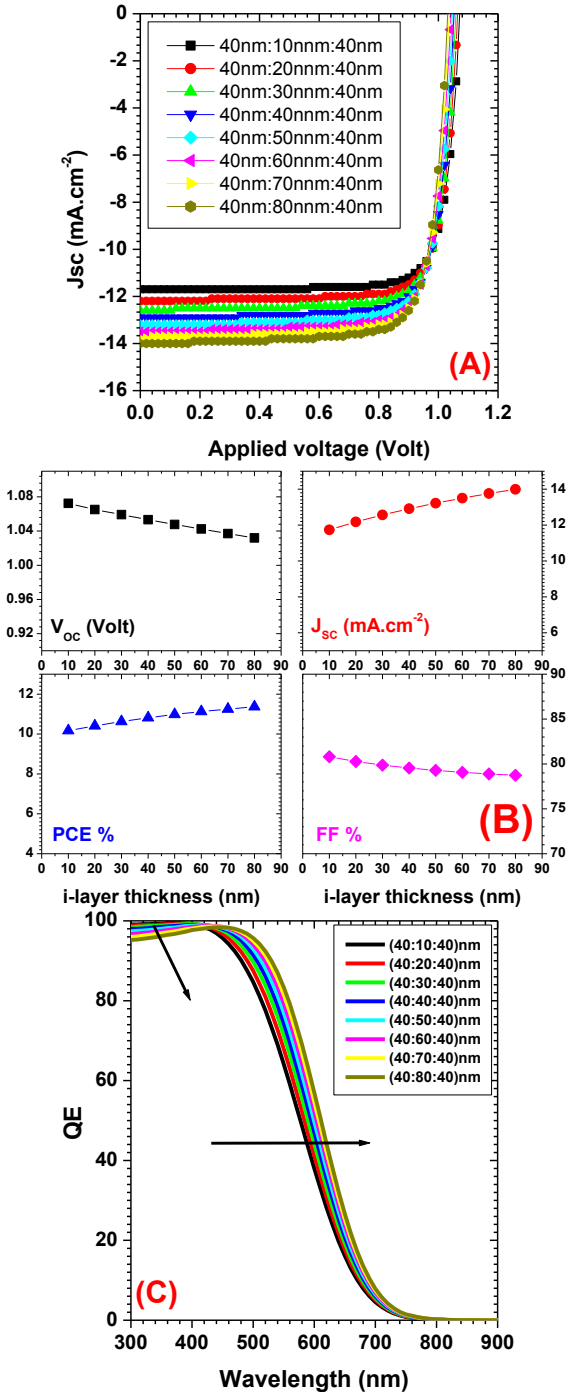

Fig. (7) Solar cell characteristics for a-Si:H-based PIN solar cell with symmetric extrinsic layers (40nm thickness and different i-layers), (A) J-V curve under illumination (B) Solar cell parameters and (C) QE

3.4. Extrinsic layer thickness (50nm)

For higher PIN thickness presented in Fig. (8), i-layer variation results in different Ef splitting inside and outside the i-layer, which suggested wider depletion region extended outside the i-layer inside both N-layer and P-layer. The i-layer thickness variation results in different depletion region as the i-layer is responsible for creating the depletion region in PIN devices [13].

Similar behavior where the E_{fn} is close to VB and E_{fp} is close to CB is observed for these samples in dark. Whereas under illumination, E_{fn} moves close to CB and E_{fp} moves close to VB.

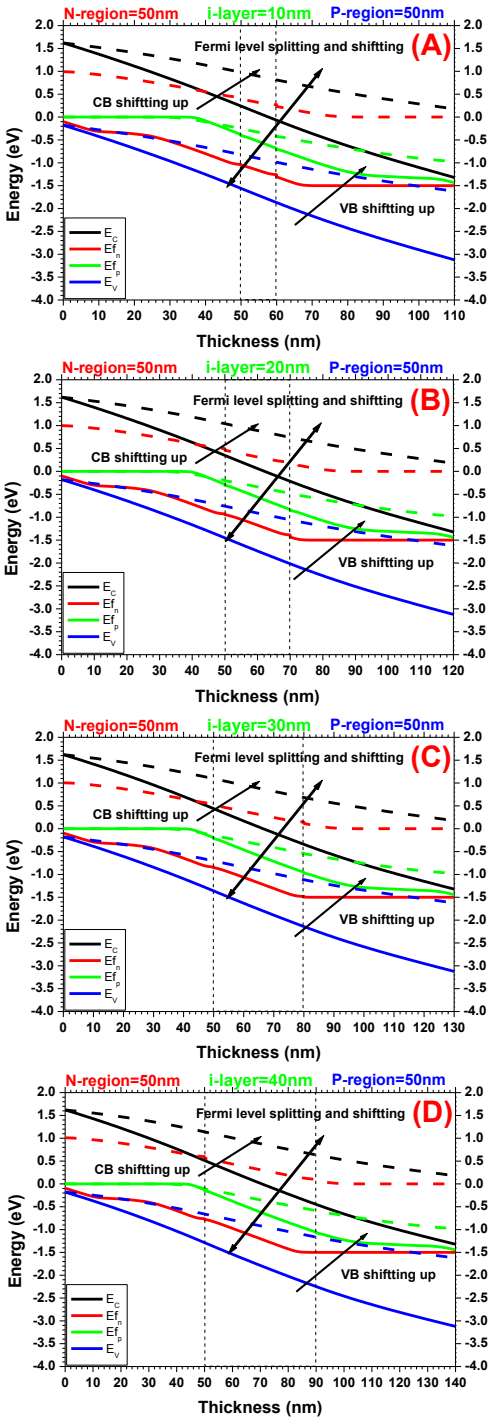

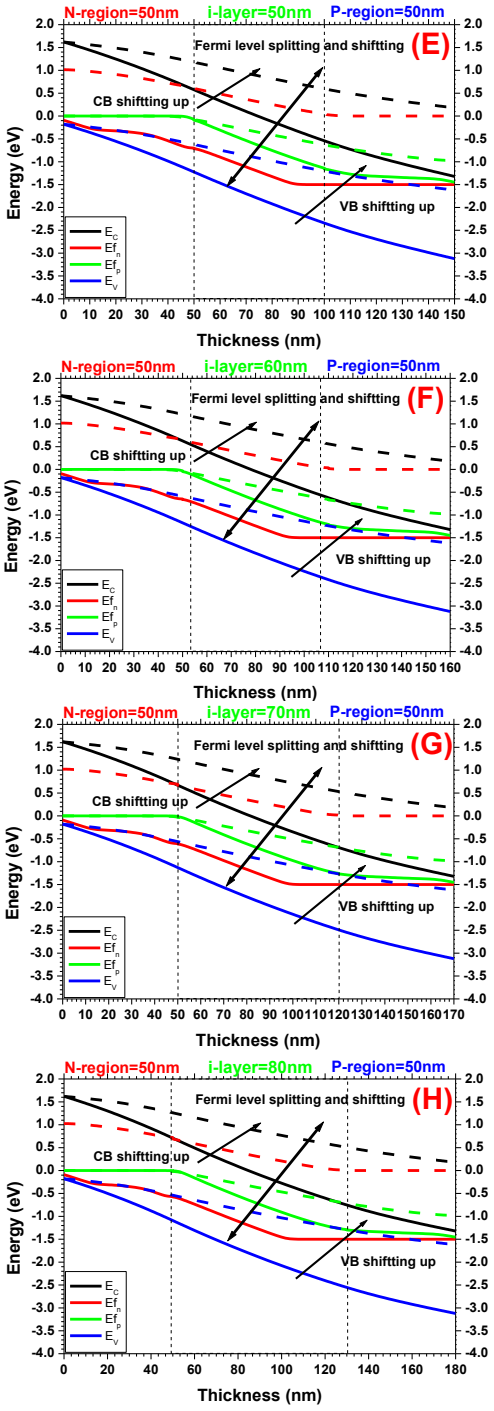

Fig. (8) Energy band alignments for a-Si:H-based PIN device that has different i-layer thickness, (A) 10nm, (B) 20nm, (C) 30 nm, (D) 40 nm, (E) 00nm, (F) 60nm, (F) 70nm and (G) 80nm with symmetric N and P-layers thickness of 50nm. Solid lines represent the energy level in dark and dash lines represent the energy level under illumination

In comparison to earlier results, the device performance is improved with V_{OC} of 1.03 V, FF of 77.1%, J_{SC} of 14.4 mA/cm^2, and PCE of 11.4% for the PIN device with a thickness of 180nm, as seen in Fig. (9A), which displays J-V curves of solar cells. QE curves in Fig. (9C) exhibit a reduction in the absorption region below 450 nm and a red shift as i-layer thickness increases. This could be explained by how the growing i-layer thickness increases light absorption [34].

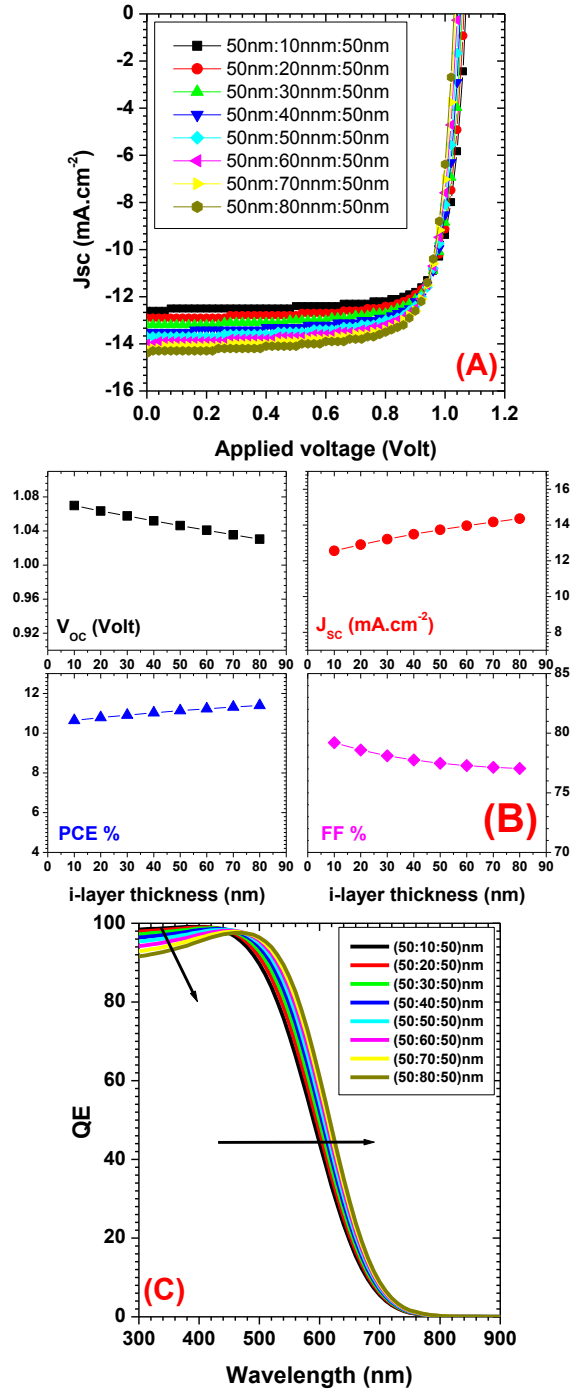

Fig. (9) Solar cell characteristics for a-Si:H-based PIN solar cell with symmetric extrinsic layers (50nm thickness and different i-layers), (A) J-V curve under illumination (B) Solar cell parameters and (C) QE

The green efficiency rises with increase of i-layer thickness, suggesting an increase in light absorption [35]. The asymmetric carrier collection phenomenon, which is particularly noticeable for short-wave light

illumination, is the reason why blue efficiency first increases and decreases after that [36]. Short-wavelength photons primarily affect a-Si:H layers, breaking Si–H bonds and reducing hydrogen content in both intrinsic and doped regions, which leads to degraded interface passivation [37]. This asymmetry refers to the uneven collection of photogenerated electrons and holes across the cell; initially, improvements in passivation and doping enhance carrier collection and blue response. Furthermore, high-energy photons are absorbed near the surface, poor passivation or carrier transport in these regions causes increased recombination and reduced efficiency [38]. For samples with thicker i-layers, this phenomenon results in a decrease in efficiency [39]. Furthermore, excessive reflection loss and mode leakage caused by 1st order diffraction, where the angle of diffraction is less than its critical angle, are responsible for the drop in the absorption region below the wavelength of 450 nm [40].

3.5. Extrinsic layer thickness (60nm)

In this section, proposing thicker extrinsic layers (60nm) results in EB alignment similar to the previous section. Changing the i-layer thickness alters the width of the depletion region, as the i-layer primarily defines this region in PIN structures [13]. In the dark, these samples show a typical pattern where E_{fn} lies near the VB, and E_{fp} is close to the CB. Under illumination, however, E_{fn} shifts toward CB and E_{fp} toward VB as shown in Fig. (10). As the extrinsic layers are higher than other samples, therefore, the depletion layer could be different and might extended inside the N and P-layers resulting in more pronounced band bending due to the higher charge distribution. Even after illumination, the band bending is shown a similar behavior.

When light is subjected to a PIN solar cell, a space charge region is created inside depletion region. This results from the interaction of the PIN solar cell's semiconductor material with incident light [41]. A space charge region is created in depletion region because of the incident light producing electron-hole pairs there. A photocurrent is produced when the electron-hole pairs are separated by electric field in space charge region [42]. Through effective collection of produced charge carriers and conversion of light energy to electrical energy, space charge region is essential to PIN solar cell's operation [43]. These devices likewise exhibit comparable behavior, with the E_{fn} close to VB and the E_{fp} close to CB. For the solar cell characteristics of these devices illustrated in Fig. (11A), the best device performance is shown in the PIN device of a thickness of 200nm as shown in Fig. (11B) with V_{OC} of 1.03 V, J_{SC} of 14.6 mA/cm^2, FF of 75%, and PCE of 11.3%. A slight decrease in the PCE is revealed which is maybe because the slight reduction in the FF, where the V_{OC} and J_{SC} are demonstrated no change in their values. The QE spectra (see Fig. 11C) shows that higher thicknesses result in red shift and the curves at low wavelengths demonstrate a decrease, this has results in increasing the current density as shown in Fig. (11B).

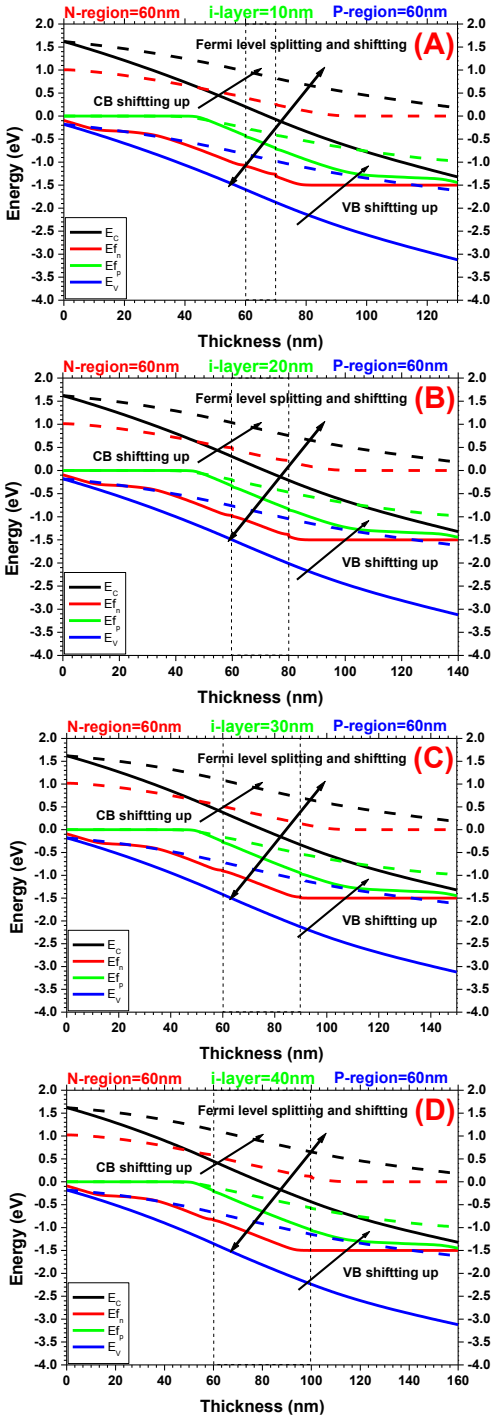

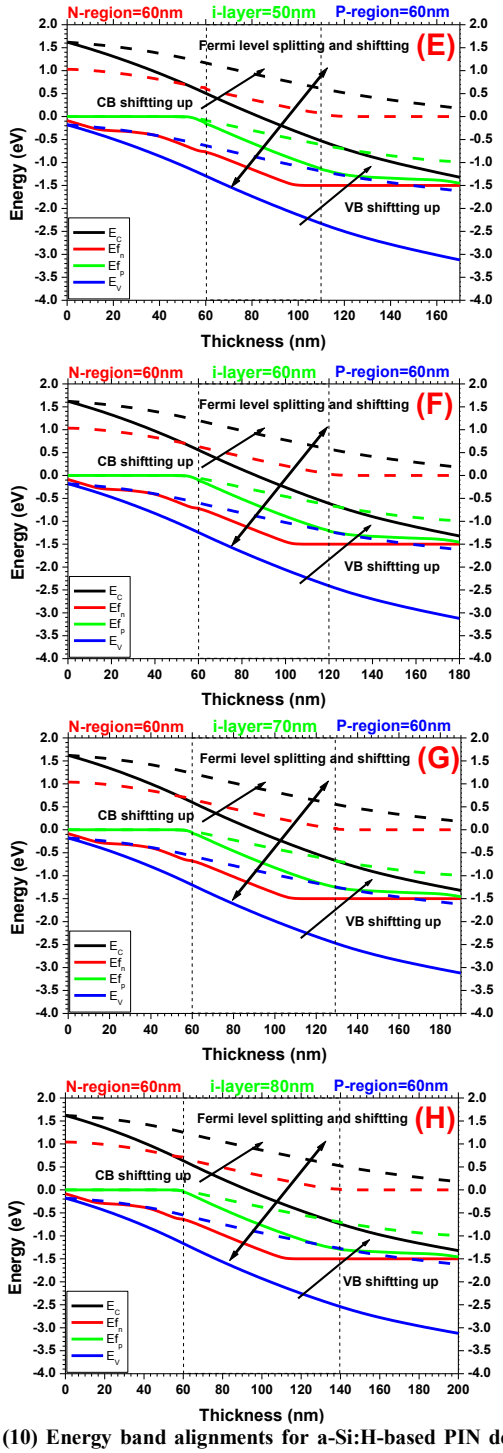

Fig. (10) Energy band alignments for a-Si:H-based PIN device with different i-layer thickness, (A) 10nm, (B) 20 nm, (C) 30nm, (D) 40 nm, (E) 00nm, (F) 60nm, (F) 70nm and (G) 80nm with symmetric N and P-layers thickness of 60nm. The solid lines represent energy level in dark and the dash lines represent the energy level under illumination

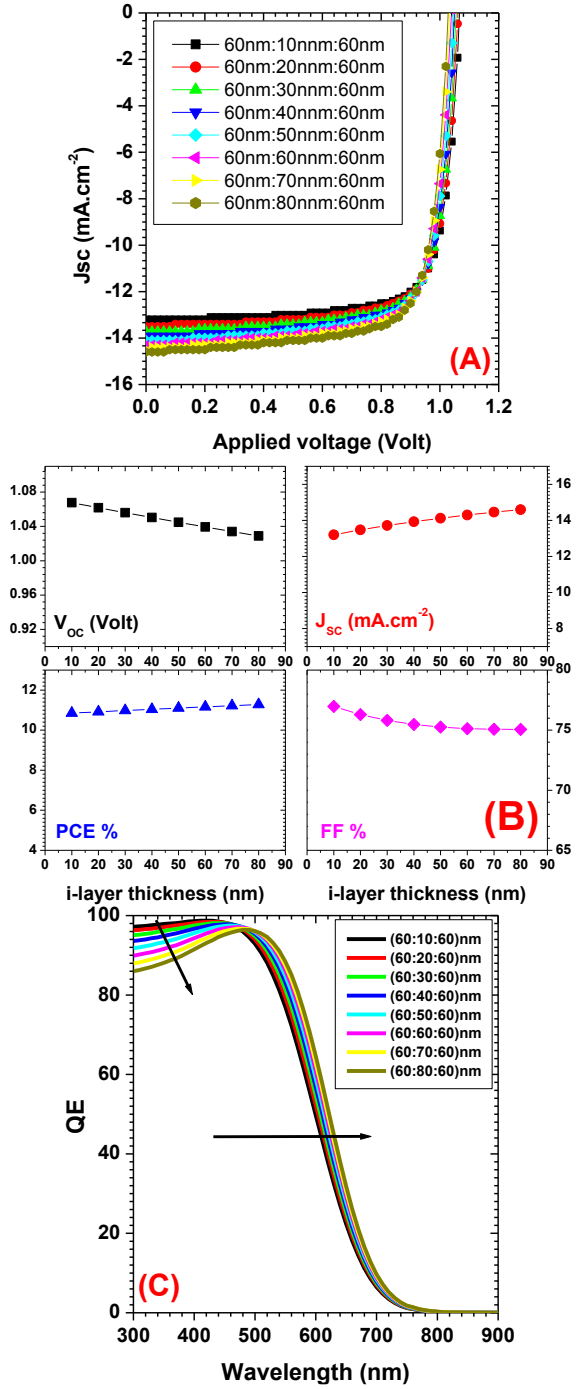

Fig. (11) Solar cell characteristics for a-Si:H-based PIN solar cell with symmetric extrinsic layers (60nm thickness and different i-layers), (A) J-V curve under illumination (B) Solar cell parameters and (C) QE

3.6. Thick PIN layer

The use of thicker PIN layer with symmetric layer thickness is suggested in this section. An a-Si solar cells are said to have a smaller depletion region than crystalline ones. Therefore, the addition of thick i-layer between thin extrinsic layers is desirable [13]. The use of thick layers results in different performance and band bending alignments as shown in Fig. (12). In dark, the gradient of CB and VC in 300nm thickness of PIN

(i-layer=100nm and extrinsic layers are 100nm each) is pronounced, even after illumination, the EB shifted up and band bending is more pronounced compare to previous results. Similar behavior where the E_{fn} is close to VB and E_{fp} is close to CB is observed for these samples in dark. However, at PIN thickness of 600nm (i-layer=200nm and extrinsic layers are 200nm each), different band bending is observed and the depletion region extended from outside the i-layer. In here, higher energy barrier is observed compared to other devices under study which may results in low performance solar cell as the low energy barrier allows smooth transport for photo-generated charge carriers [44]. The band bending creates barrier in the region starting from 100nm to 600nm in Fig. (12B) compare to smooth gradient in Fig. (12A) starting from 20nm to 280nm. This bending results in charge barriers. Moreover, this bending is clearly increased in Fig. (12C-E) in the regions 200nm-700nm, 260nm-850nm, and 500nm-1100nm, respectively. Authors believe that these results could give a deep insight of the band structure in dark and under illumination towards fabricating flexible a-Si solar cell. Thin layers are essential for flexible application and the optimization of the device parameters is needed. The solar cell characteristics shown in Fig. (13A) are demonstrate different behavior compare to previous devices. Results are revealed that the PIN solar cell with thickness of 300nm (P=100nm/i=100nm/N=100nm) exhibited the best device performance compare to other thick devices with V_{OC} of 1.01 V, J_{SC} of 14.04 mA/cm^2, FF of 71.7% and PE of 10.2%, while thicker device (P=500nm/i=500nm/N=500nm) results in decreasing all the solar cell parameters as exhibited in Fig. (13B). The devices exhibit high absorption at wavelengths above 550 nm, yet the absorption below this wavelength is drastically reduced, which directly affects the current density. The reduction in J_{SC} is approximately 50%, which is correlated with the reduction in QE spectra. The results are displayed in Fig. (13C).

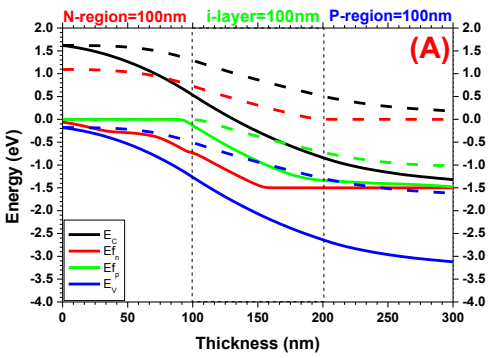

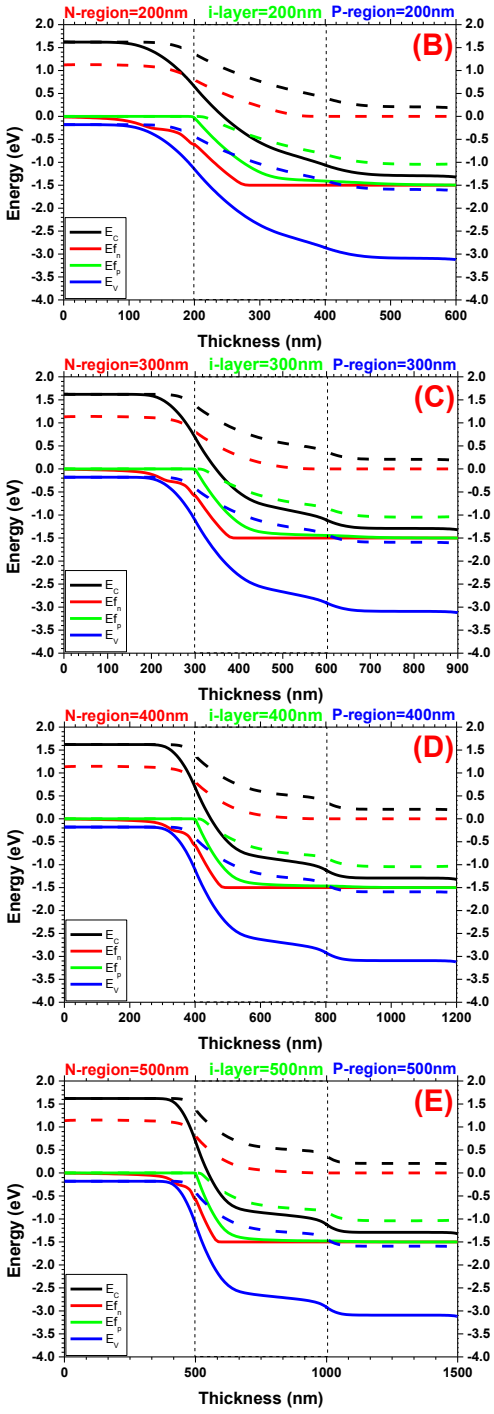

Fig. (12) Energy band alignments for a symmetric a-Si:H-based PIN device, (A) N, i and P-layer is 100nm (B) N, i and P-layer is 200nm (C) N, i and P-layer is 300nm, (D) N, i and P-layer is 400nm and (E) N, i and P-layer is 500nm. The solid lines represent energy level in dark and the dash lines represent energy level under illumination

The asymmetric carrier collection phenomenon, which is particularly noticeable for short-wave light illumination, is responsible for the blue efficiency's initial increase and subsequent decline [36]. For samples with thicker i-layers, this phenomenon results in a decrease in efficiency [39]. Furthermore, excessive

reflection loss and mode leakage that are caused by 1st order diffraction, where the angle of diffraction is less than the critical angle, are responsible for the drop in the absorption region below the wavelength of 450 nm [40].

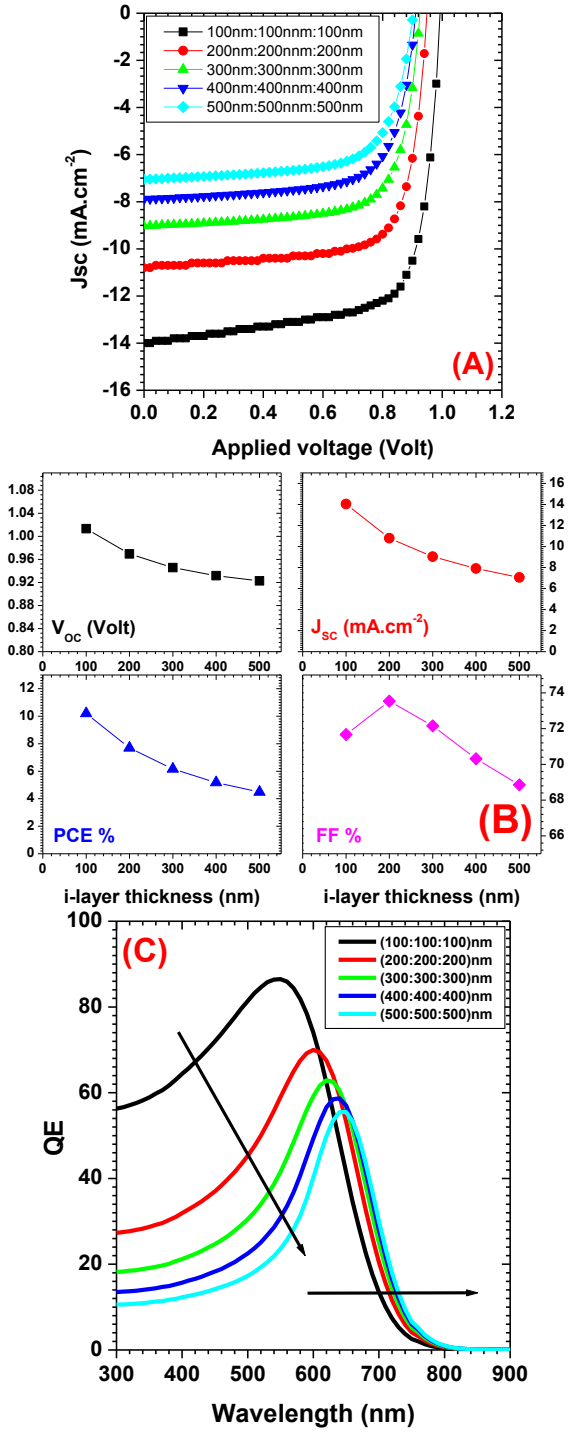

Fig. (13) Solar cell characteristics for a-Si:H-based PIN solar cell with symmetric thickness of extrinsic and intrinsic layers, (A) J-V curve under illumination (B) Solar cell parameters and (C) QE

4. Conclusion

The current study focuses on the effects of intrinsic layer in PIN solar cells based on amorphous Si using SCAPS-1D software. The results are promising and reflect a strong and effective understanding of the energy band alignment in PIN layers under both dark and illuminated conditions. Results show that thin amorphous Si could be fabricated, however, a careful engineering must take into account during the fabrication to overcome the possible loss in the charge carriers and the output of the solar cells. The overlapping and splitting of Fermi level for electrons and holes is affected by intrinsic and extrinsic layers' thickness. Results also show that higher PIN thickness is not favorable for amorphous Si solar cell due to the high energy barrier created. The solar cell with a thickness of 180 nm (i = 80 nm, N = 50 nm, and P = 50 nm) and a J_{SC} of 14.4 mA/cm^2, open circuit voltage of 1.03 V, an FF of 77.1%, and a PCE of 11.4% is shown to have the best performance. The performance of thicker PIN solar cells is obviously decreased.

References

[1] W. Liu et al., "Flexible solar cells based on foldable silicon wafers with blunted edges", *Nature,* 617(7962) (2023) 717-723.

[2] F. Meillaud et al., "Recent advances and remaining challenges in thin-film silicon photovoltaic technology", *Mater. Today,* 18(7) (2015) 378-384.

[3] C.-L. Lin et al., "Gate driver based on a-Si: H thin-film transistors with two-step-bootstrapping structure for high-resolution and high-frame-rate displays", *IEEE Trans. Electron Dev.,* 64(8) (2017) 3494-3497.

[4] L. Lin et al., "Mesoporous Amorphous silicon: a simple synthesis of a high-rate and long-life anode material for lithium-ion batteries", *Angewandte Chemie,* 128(45) (2016) 14269-14272.

[5] W. Liu et al., "Damp-heat-stable, high-efficiency, industrial-size silicon heterojunction solar cells", *Joule,* 4(4) (2020) 913-927.

[6] A. Al-Ashouri et al., "Monolithic perovskite/silicon tandem solar cell with> 29% efficiency by enhanced hole extraction", *Science,* 370(6522) (2020) 1300-1309.

[7] S. Kugler et al., "Structure of evaporated pure amorphous silicon: Neutron-diffraction and reverse Monte Carlo investigations", *Phys. Rev. B,* 48(10) (1993) 7685.

[8] J. Ramanujam et al., "Flexible CIGS, CdTe and a-Si: H based thin film solar cells: A review", *Prog. Mater. Sci.,* 110 (2020) 100619.

[9] J. Merten et al., "Improved equivalent circuit and analytical model for amorphous silicon solar cells and modules", *IEEE Trans. Electron Dev.,* 45(2)

(1998) 423-429.
[10] Y. Wang et al., "Modeling method research of flexible amorphous silicon solar cell", *Appl. Solar Energy,* 51 (2015) 41-46.
[11] J. Cubas, S. Pindado and C. De Manuel, "Explicit expressions for solar panel equivalent circuit parameters based on analytical formulation and the Lambert W-function", *Energies,* 7(7) (2014) 4098-4115.
[12] R. Yang et al., "Flexible semi-transparent a-Si: H pin solar cells for functional energy-harvesting applications", *Mater. Sci. Eng. B,* 229 (2018) 1-5.
[13] I. Benigno and D. Darminto, "Effect of intrinsic layer energy gap and thicknesses optimization on the efficiency of pin amorphous silicon solar cell", *IPTEK J. Sci.*, 2(3) (2017) 37-42.
[14] L. Ayat and A. Idda, "Analysis of a-Si: H/SiGe heterostructure solar cell", *J. Ovonic Res.,* 19(2) (2023) 165-173.
[15] M. Belarbi, O. Zeggai and S. Louhibi-Fasla, "Parameters optimization of heterojunction ZnSe/CdS/CIGS/Si solar cells using SCAPS-1D software", *J. Renew. Ener.,* (2022) 31-36.
[16] G.S. Sahoo and G.P. Mishra, "Use of hetero intrinsic layer in GaAs PIN solar cell to improve the intermediate band performance", *Mater. Sci. Eng. B,* 263 (2021) 114862.
[17] L. Mousli, B. Dennai and B. Azeddine, "The effect of molar fraction of the intrinsic layer on the PIN structure for solar cell based on indium gallium nitride using AMPS-1D", *J. Optoelectron. Adv. Mater.,* 73(7) (2021) 2235-2240.
[18] J.-P. Yang, H.-T. Chen and G.-B. Tang, "Modeling of thickness-dependent energy level alignment at organic and inorganic semiconductor interfaces", *J. Appl. Phys.,* 131(24) (2022) 245501.
[19] G.T. Yue et al., "Flexible dye-sensitized solar cell based on PCBM/P3HT heterojunction", *Chinese Sci. Bull.,* 56 (2011) 325-330.
[20] W. Ma et al., "Thermally stable, efficient polymer solar cells with nanoscale control of the interpenetrating network morphology", *Adv. Func. Mater.,* 15(10) (2005) 1617-1622.
[21] B.Y. Kadem, A.K. Hassan and W. Cranton, "Enhancement of power conversion efficiency of P3HT: PCBM solar cell using solution processed Alq_3 film as electron transport layer", *J. Mater. Sci.: Mater. Electron.,* 26 (2015) 3976-3983.
[22] K. Shiba, Y. Okada and T. Sogabe, "Drift–Diffusion Simulation of Intermediate Band Solar Cell: Effect of Intermediate Band Continuity Constraint", *J. Nanomater.,* 2023(1) (2023) 5578627.
[23] K. Nagata et al., "Visualization of depletion layer in AlGaN homojunction p–n junction", *Appl. Phys. Exp.,* 15(3) (2022) 036504.
[24] F. Mortreuil et al., "Influence of dielectric layer thickness on charge injection, accumulation and transport phenomena in thin silicon oxynitride layers: a nanoscale study", *Nanotech.,* 32(6) (2020) 065706.
[25] X. Liu et al., "Fermi level pinning dependent 2D semiconductor devices: challenges and prospects", *Adv. Mater.,* 34(15) (2022) 2108425.
[26] A. Hankin et al., "Flat band potential determination: avoiding the pitfalls", *J. Mater. Chem. A,* 7(45) (2019) 26162-26176.
[27] H. Kaur et al., "Electrical characteristics analysis of PIN detector with different doping concentration levels of N and P-type materials", *Mater. Today: Proc.,* 28 (2020) 1879-1886.
[28] F. Cao, M. Wang and L. Li, "Graded energy band engineering for efficient perovskite solar cells", *Nano Select,* 1(2) (2020) 152-168.
[29] M. Al-Hashimi et al., "The effects of solvent treated PEDOT: PSS buffer layer in organic solar cells", *J. Mater. Sci.: Mater. Electron.,* 29 (2018) 13889-13896.
[30] A. Hassan, B. Kadem and W. Cranton, "Organic solar cells: Study of combined effects of active layer nanostructure and electron and hole transport layers", *Thin Solid Films,* 636 (2017) 760-764.
[31] I.A. Yunaz et al., "Wide-gap a-$Si_{1-x}C_x$:H solar cells with high light-induced stability for multijunction structure applications", *Sol. Eener. Mater. Sol. Cells,* 95(1) (2011) 107-110.
[32] M. Fischer et al., "Degradation kinetics of amorphous silicon solar cells processed at high pressure and its relation to the nanostructure", in 2013 IEEE 39th Photovoltaic Specialists Conference (PVSC) PART 2, pp. 045-049.
[33] B.Y. Kadem et al., "The effects of the PEDOT: PSS acidity on the performance and stability of P3HT: PCBM-based OSCs", *J. Mater. Sci.: Mater. Electron.,* 29 (2018) 19287-19295.
[34] R.J. Koval et al., "Evolution of the mobility gap with thickness in hydrogen-diluted intrinsic Si: H materials in the phase transition region and its effect on pin solar cell characteristics", *MRS Online Proc. Library (OPL),* 664 (2001) A16-4.
[35] K. Belrhiti Alaoui et al., "Photovoltaic and impedance spectroscopy characterization of single-junction a-Si: H p–i–n solar cells deposited by simple shadow masking techniques using PECVD", *AIP Adv.,* 10(9) (2020).
[36] R.Y. Zhang et al., "Absorption enhancement analysis of crystalline Si thin film solar cells based on broadband antireflection nanocone grating", *J. Appl. Phys.,* 110(11) (2011) 113105.
[37] H. Ye et al., "Short Wavelength Photons Destroying Si–H Bonds and Its Influence on High-Efficiency Silicon Solar Cells and Modules", *Solar RRL*, 7(15) (2023) 2300334.

[38] R.S. Bonilla et al., "Dielectric surface passivation for silicon solar cells: A review", *phys. stat. sol. (a)*, 214(7) (2017) 1700293.
[39] S. Jiyue et al., "P-3.4: Strategies to Improve the Photoelectric Performance of a-Si: H pin Ambient Light Sensor", in SID Symposium Digest of Technical Papers, vol. 53(S1) (2022) pp. 682-682.
[40] S. Prayogi et al., "The effect of adding an active layer to the structure of a-Si: H solar cells on the efficiency using RF-PECVD", *J. Mater. Sci.: Mater. Electron.,* 32(6) (2021) 7609-7618.
[41] J.G. Tait et al., "Interfacial depletion regions: beyond the space charge limit in thick bulk heterojunctions", *ACS Appl. Mater. Interfaces,* 8(3) (2016) 2211-2219.
[42] A.N.R. Choudhury, "PIN Solar Cell Characteristics: Fundamental Physics", in Mathematical Modeling for Intelligent Systems (2022), Chapman and Hall/CRC, pp. 119-132.
[43] K. Keya et al., "Correlation between SiH_2/SiH and light-induced degradation of p–i–n hydrogenated amorphous silicon solar cells", *Japanese J. Appl. Phys.,* 55(7S2) (2016) 07LE03.
[44] X. Li et al., "Roll-over behavior in current-voltage curve introduced by an energy barrier at the front contact in thin film CdTe solar cell", *Solar Energy,* 165 (2018) 27-34.

